Intensity based measuring of the topological charge alteration by the diffraction of vortex beams from amplitude sinusoidal radial gratings

DAVUD HEBRI[1], SAIFOLLAH RASOULI[1,2,*], AND MOHAMMAD YEGANEH[1]

[1] Department of Physics, Institute for Advanced Studies in Basic Sciences (IASBS), Zanjan 45137-66731, Iran
[2] Optics Research Center, Institute for Advanced Studies in Basic Sciences (IASBS), Zanjan 45137-66731, Iran.
[*] Corresponding author: rasouli@iasbs.ac.ir

Compiled January 27, 2018

For convenient optical communications by the aid of vortex beams, topological charge alterations should be translated to the change in intensity of the output light. In this paper, we formulate and experimentally investigate diffraction of vortex beams from amplitude radial gratings having sinusoidal profile. We show that, the diffraction pattern simply renders both topological charge and twist direction of the impinging vortex beam. When, topological charge of the vortex beam and the radial grating spokes number are equal, intensity on the optical axes of the Fraunhofer pattern gets a maximum value. Otherwise, its value on the optical axes remains zero. We examined the method on different vortex beams, the measured topological charge of generated beams are in an excellent agreement with the excepted values. We show that an alteration between two vortex beams, in which one has a topological charge of equal to the grating spokes number, is translated to a binary change in intensity of the output light on the optical axes. This feature might find wide applications in optical communications.

OCIS codes: (050.4865) Optical vortices ; (050.0050) Diffraction and gratings; (260.6042) Singular optics, topological defects; (060.4510) Optical communications.

http://dx.doi.org/10.1364/ao.XX.XXXXXX

1. INTRODUCTION

As optical vortex beams carry orbital angular momentum, they are used in trapping, manipulation, and transferring of angular momentum to small particles [1], optical communications [2], quantum state manipulation [3], and so on. Due to these features, they have garnered great deal of attention in recent years. A number of methods have been proposed to determine the topological charge (TC) of an incident vortex beam, including interferometry [4], moiré deflectometry [5], Talbot effect [6] and diffraction from gratings [7–9], and the use of optical elements such as an annular aperture [10], an axicon [11], a wedged optical flat [12], a sectorial screen [13], phase shift devices [14], and so on. Furthermore, a considerable number of researches are dedicated to the use of vortex beams in optical communications [2, 15, 16].

We have recently investigated diffraction of a plane wave from amplitude radial gratings and we observed unprecedented optical patterns at the transverse planes that are shape-invariant during propagation [17]. In that work, we have shown that the geometric shadow and near-field and far-field diffraction patterns are observable at planes parallel to the grating plane and are continuous at distances from the grating. Also, a resulting pattern was interpreted as the Talbot carpet at the transverse plane. Most importantly, in that work we have shown that, as a consequence of turning a conventional grating into a radial grating with a central singularity, the plane boundaries between the optical regimes have acquired curvature.

It is worth mentioning that in another work, an introductory study of the diffraction of plane wave from radial rings was presented [18]. In that work, although experimental results of diffraction from amplitude radial gratings were presented, the observed phenomenon has been interpreted wrongly. In that work, there is no address to the fine structure of the resulting diffraction patterns in the transverse planes, such as the formation of sub-images, half-images, transverse Talbot carpet, and to the fact that in this type of diffraction, the geometric shadow, and the near-field and far-field diffraction regimes are mixed at various propagation distances. At the same time, the designation of the diffraction pattern on the transverse plane as the self-image of the radial grating is incorrect, and the use of dark fringes is meaningless. In another work, the diffraction of a Gaussian beam from an out-of-center portion of an amplitude radial grating has been previously considered and an evolution

for the spatial profile of the beam was reported [19, 20]. Finally, it is worth remembering that, we have recently presented a simple and comprehensive method by the aid of reciprocal vector approach to take into account the central singularity and any additional out-of-center singularities of the radial gratings in formulating their structures and we have investigated the moiré patterns of radial gratings consisting of out-of-center singularities [21].

To the best of our knowledge, the diffraction of vortex beams from radial gratings has not been considered in the literature so far. In the following we consider a very interesting subject, the fusion of the Fresnel and Fraunhofer diffraction properties with singular optics. Here we show that, by using a vortex beam instead of a plane wave, the behaviour of diffraction patterns remarkably changes. In this paper, a novel and reliable method for determining the TC of vortex beams by diffraction from amplitude radial gratings is reported. Also, we propose a convenient optical communication method by translating the TC alteration in intensity change.

2. PROPAGATION OF A LIGHT BEAM WITH AN INITIAL COMPLEX AMPLITUDE SEPARABLE IN THE POLAR COORDINATES

First, propagation of a light beam having complex amplitude with a separable functionality in the polar coordinates is reviewed [17]. We consider $\psi(r',\theta';0)$ as the complex amplitude of the light field at input plane $(z=0)$, and $\psi(r,\theta;z)$ as the resulted complex amplitude after a propagation distance of z, in which (r',θ') and (r,θ) indicate polar coordinates on the input and output planes, respectively. Separability of the complex amplitude at $z=0$ can be shown by

$$\psi(r',\theta';0) = f(r')\,g(\theta'). \tag{1}$$

As $g(\theta')$ is an inherently periodic function with the period 2π, it can be expanded by using Fourier series as

$$g(\theta') = \sum_{n=-\infty}^{+\infty} g_n e^{in\theta'}, \tag{2}$$

where g_n are the Fourier series coefficients. Now let us recall definition of Hankel transform order n of $f(r)$ [22]

$$\mathcal{H}_n\{f(r)\} = 2\pi \int_0^{+\infty} f(r) J_n(2\pi\rho r) r dr, \tag{3}$$

where J_n is the nth Bessel function of the first kind. By using Fresnel integral we can show that [17]

$$\psi(r,\theta;z) = h_0 e^{i\alpha r^2} \sum_{n=-\infty}^{+\infty} g_n (-i)^n e^{in\theta} \mathcal{H}_n\{f(r) e^{i\alpha r^2}\}, \tag{4}$$

where $h_0 = \frac{1}{iz\lambda}\exp(ikz)$ and $\alpha = \frac{\pi}{z\lambda}$, in which λ is the wavelength of the light beam and $k = \frac{2\pi}{\lambda}$ is the wave-number. Moreover after getting Hankel transform we should set $\rho = \frac{r}{\lambda z}$. Eq. 4 stands in the near-field diffraction regime. In the Fraunhofer approximation, Eq. 4 reduces to [22]

$$\psi(r,\theta;z) = h_0 \sum_{n=-\infty}^{+\infty} g_n (-i)^n e^{in\theta} \mathcal{H}_n\{f(r)\}. \tag{5}$$

As is apparent from Eqs. 4 and 5, the separability of the initial complex amplitude is violated by the propagation.

3. NEAR- AND FAR-FIELD DIFFRACTION OF A VORTEX BEAM FROM A SINUSOIDAL RADIAL AMPLITUDE GRATING

Now, we use the above-presented formulation for the diffraction of a vortex beam from an amplitude radial grating having sinusoidal profile in the near- and far-field regimes. Complex amplitude of an optical vortex beam with an order l can be written by

$$\psi(r,\theta,-0) = (\frac{r}{w})^{|l|} \exp\left[-(\frac{r}{w})^2 + il\theta\right], \tag{6}$$

where w is the vortex beam radius parameter in which the maximum value of the intensity is located at an effective radius of $w_{eff} = w\sqrt{\frac{|l|}{2}}$. This vortex beam passes through an amplitude radial grating with a sinusoidal transmission profile of

$$t(r,\theta) = \frac{1}{2}[1+\cos(m\theta)], \tag{7}$$

where m is the number of spokes of the grating. Complex amplitude immediately after the grating can be written by

$$\psi(r,\theta,+0) = t(r,\theta)\,\psi(r,\theta,-0), \tag{8}$$

where -0 and $+0$ signify immediately before and after the grating, respectively (see Fig. 1). Then we can obtain

$$\psi(r,\theta,+0) = \frac{1}{4}(\frac{r}{w})^{|l|} e^{-(\frac{r}{w})^2}(2e^{il\theta} + e^{i(m+l)\theta} + e^{-i(m-l)\theta}). \tag{9}$$

As $\psi(r,\theta,+0)$ is separable in the polar coordinates, by comparing with Eqs. 1 and 2 we conclude that $f(r) = \frac{1}{4}(\frac{r}{w})^{|l|} e^{-(\frac{r}{w})^2}$, $g_l = 2$, $g_{m+l} = g_{-(m-l)} = 1$, and other coefficients are zero. By

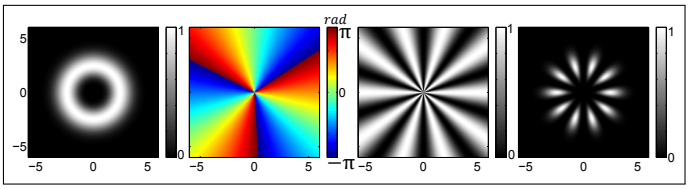

Fig. 1. From left: intensity and phase patterns of a typical vortex beam with $l=+3$ and $w=2mm$, transmission profile of a radial grating with $m=10$, and transmitted intensity of the vortex beam after the grating. All lengths are in millimeters.

using Eq. 4, we have

$$\psi(r,\theta,z) = h_0\, e^{i(\alpha r^2 + l\theta)} \times\{2(-i)^{|l|} H_{|l|} + (-i)^{m+l} e^{im\theta} H_{m+l} + (-i)^{m-l} e^{-im\theta} H_{m-l}\}, \tag{10}$$

where $H_{|l|} = \mathcal{H}_{|l|}\{f(r)e^{i\alpha r^2}\}$, $H_{m\pm l} = \mathcal{H}_{m\pm l}\{f(r)e^{i\alpha r^2}\}$, and following identity:

$$\mathcal{H}_{-n}\{f(r)\} = (-1)^n \mathcal{H}_n\{f(r)\}, \tag{11}$$

is used. By defining $\gamma = \frac{1}{w^2} - i\alpha$ we get

$$f(r)e^{i\alpha r^2} = \frac{1}{4}(\frac{r}{w})^{|l|} e^{-\gamma r^2}. \tag{12}$$

Now, using Hankel transform definition, Eq. 3, we have

$$H_{|l|} = \frac{\pi}{2w^{|l|}} \int_0^{\infty} r^{|l|+1} e^{-\gamma r^2} J_{|l|}(2\pi\rho r) dr, \tag{13}$$

and using the following integral [23]:

$$\int_0^\infty x^{\nu+1}e^{-ax^2}J_\nu(bx)dx = \frac{b^\nu}{(2a)^{\nu+1}}e^{-\frac{b^2}{4a}}, \tag{14}$$

$H_{|l|}$ can be calculated as

$$H_{|l|} = \frac{1}{4\rho w^{|l|}}\left(\frac{\pi\rho}{\gamma}\right)^{|l|+1}e^{-\frac{\pi^2\rho^2}{\gamma}}. \tag{15}$$

Now again, by using Hankel transform definition and Eq. 12 we have

$$H_{m\pm l} = \frac{\pi}{2w^{|l|}}\int_0^\infty r^{|l|+1}e^{-\gamma r^2}J_{m\pm l}(2\pi\rho r)dr, \tag{16}$$

and using the following integral [23]:

$$\int_0^\infty x^\mu e^{-ax^2}J_\nu(bx)dx = \frac{\Gamma(\frac{\nu+\mu+1}{2})e^{-\frac{b^2}{8a}}}{ba^{\frac{\mu}{2}}\Gamma(\nu+1)}M_{\frac{\mu}{2},\frac{\nu}{2}}\left(\frac{b^2}{4a}\right), \tag{17}$$

where M indicates Whittaker function, $H_{m\pm l}$ is calculated as

$$H_{m\pm l} = \frac{e^{-\frac{\pi^2\rho^2}{2\gamma}}G_\pm}{4\rho w^{|l|}\gamma^s}M_{s,\frac{m\pm l}{2}}\left(\frac{\pi^2\rho^2}{\gamma}\right), \tag{18}$$

in which $s = \frac{|l|+1}{2}$ and $G_\pm = \frac{\Gamma(\frac{|l|+m\pm l+2}{2})}{\Gamma(m\pm l+1)}$. By substituting $H_{|l|}$ and $H_{m\pm l}$ in Eq. 10 we get

$$\psi(r,\theta,z) = \tag{19}$$
$$\psi_N \times \{2(-i)^{|l|}R^s e^{-\frac{R}{2}} + \Gamma_+ M_{s,\frac{m+l}{2}}(R) + \Gamma_- M_{s,\frac{m-l}{2}}(R)\},$$

where $R = \frac{\pi^2\rho^2}{\gamma} = \frac{1}{\gamma}(\frac{\pi r}{\lambda z})^2$ is a dimensionless complex parameter, $\Gamma_\pm = (-i)^{m\pm l}e^{\pm im\theta}G_\pm$, and $\psi_N = \frac{e^{i(ar^2+l\theta+kz)}e^{-\frac{R}{2}}}{4irw^{|l|}\gamma^s}$. As Gamma functions is not defined for the negative integers, the last equation is valid when $|l| \le m$. For the case $l > m > 0$ similarly we can get

$$\psi(r,\theta,z) = \tag{20}$$
$$\psi_N \times \{2(-i)^{|l|}R^s e^{-\frac{R}{2}} + \Gamma'_+ M_{s,\frac{l+m}{2}}(R) + \Gamma'_- M_{s,\frac{l-m}{2}}(R)\},$$

where $\Gamma'_\pm = \frac{\Gamma(2s\pm\frac{m}{2})}{\Gamma(2s\pm m)}(-i)^{l\pm m}e^{\pm im\theta}$. As well as, when $l < -m < 0$ we can get

$$\psi(r,\theta,z) = \tag{21}$$
$$\psi_N \times \{2(-i)^{|l|}R^s e^{-\frac{R}{2}} + \Gamma''_+ M_{s,\frac{|l|-m}{2}}(R) + \Gamma''_- M_{s,\frac{|l|+m}{2}}(R)\},$$

where $\Gamma''_\pm = \frac{\Gamma(2s\mp\frac{m}{2})}{\Gamma(2s\mp m)}(-i)^{|l|\mp m}e^{\pm im\theta}$. Finally for the case $l = 0$, Eq. 19 reduces to

$$\psi(r,\theta,z) = \psi_N \times \left[R^{\frac{1}{2}}e^{-\frac{R}{2}} + \Gamma_0 M_{\frac{1}{2},\frac{m}{2}}(R)\cos(m\theta)\right], \tag{22}$$

where $\Gamma_0 = \frac{\Gamma(\frac{m}{2}+1)}{\Gamma(m+1)}(-i)^m$. At far-field regime only by replacing R by a real dimensionless parameter $R' = (\pi w\rho)^2 = (\frac{\pi wr}{\lambda z})^2$ and ψ_N by $\psi_F = \frac{e^{i(l\theta+kz)}}{4i}(\frac{w}{r})e^{-\frac{R'}{2}}$ same Eqs. of 19 – 22 can be used.

Let us recall the Talbot distance of the conventional gratings that is given by $z_T = \frac{2p^2}{\lambda}$ where p indicates period of the structure. In analogy, for a radial grating illuminated by a vortex beam with an effective radius of w_{eff}, we can define a spatial period in the angular direction over the illuminated area by $p = \frac{2\pi w_{eff}}{m}$. Therefore based on this angular periodicity and using $w_{eff} = w\sqrt{\frac{|l|}{2}}$, we get

$$z_T = \frac{|l|}{\lambda}\left(\frac{2\pi w}{m}\right)^2 = \frac{|l|}{m^2}z_0, \tag{23}$$

where $z_0 = \frac{(2\pi w)^2}{\lambda}$. z_T can be considered as a characteristic distance for the Fresnel diffraction from a radial grating. More details on the definition of z_T for radial gratings can be found in [17].

For an amplitude radial grating with $m = 10$ illuminated by beams having $l = 0, \pm 3$, the calculated intensity patterns immediately after the grating and their corresponding near-field diffraction patterns at a propagation distance equal to z_T are illustrated in Fig. 2. As is apparent, for the cases of the vortex beams, spokes on the diffraction patterns experience a deflection and get a spiral-like forms. For each of these cases, the deflection direction depends on the twist direction (TD) of the vortex beam.

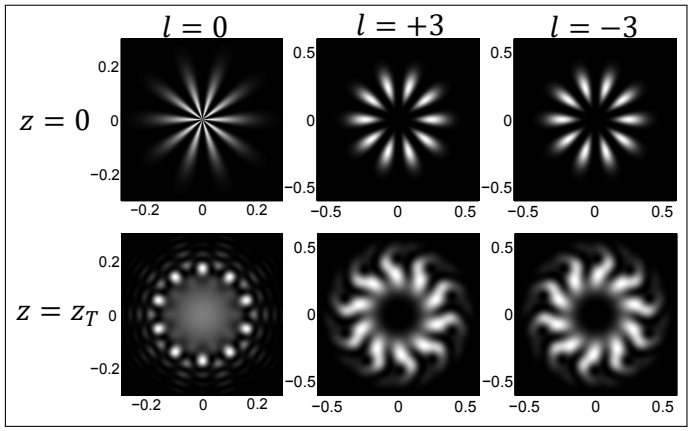

Fig. 2. First row: intensity patterns immediately after an amplitude radial grating with $m = 10$ illuminated by vortex beams of $l = 0, \pm 3$. Second row: corresponding calculated near-field diffraction patterns at the propagation distinct of z_T. All lengths are in millimeters (see Visualization 1).

In Fig. 3, calculated near-field diffraction patterns for an amplitude radial grating having $m = 15$ illuminated by vortex beams of $l = \pm 10, \pm 14, \pm 15$, and ± 16 at a propagation distinct of $2z_T$ are shown. Here again, deflection direction of the spokes determines the TD of the impinging optical vortex beam. In addition, we see that on the optical axis the intensity has zero values for all $l \neq \pm m$ and only for $l = \pm m$ its value switches to a locally maximum value.

All aspects of the presented work are demonstrated in Visualization 1. It presents the calculated diffraction patterns from an amplitude radial grating with $m = 10$ illuminated by the vortex beams with $w = 2mm$ and $l = \pm 3, \pm 10$ at different propagation distances in the range from $z = 0$ to $z = 10z_T$. For the cases $m = |l| = 10$ by propagation, the beams' energy are flowing towards the optical axes and as a consequence the intensity value becomes absolute maximum on the optical axis at the far-field regime. All dimensions are in millimeters.

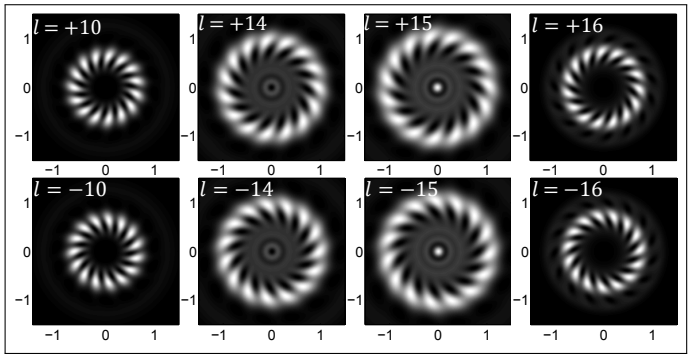

Fig. 3. Near-field diffraction patterns of an amplitude radial grating with $m = 15$ illuminated by vortex beams of $l = \pm 10, \pm 14, \pm 15$, and ± 16 at the propagation distinct of $2z_T$ (see Visualization 1). Plot shows their intensity profiles. All lengths are in millimeters.

Fig. 4 shows calculated and experimentally recorded Fraunhofer diffraction patterns from two amplitude radial gratings with $m = 5, 10$ illuminated by vortex beams having various l. Here, we present these experimentally recorded patterns for a better comparing with the corresponding calculated patterns. The details concerning experimental patterns will be presented in Section 4. As is apparent, far-field diffraction patterns are not sensitive to the TD but in this regime on the optical axis the intensity value for each of pattern when $|l| = m$ is maximized and for the other cases its value is zero.

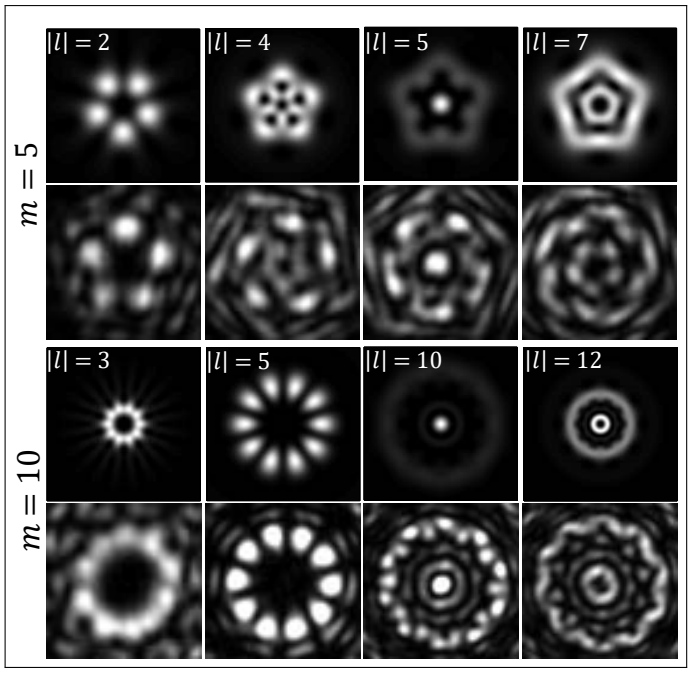

Fig. 4. Calculated (first and third rows) and corresponding experimentally recorded (second and forth rows) Fraunhofer diffraction patterns from two amplitude radial gratings with $m = 5, 10$ illuminated by vortex beams having different values of l (see Visualization 1).

Therefore here again, we show that when the topological charge of the vortex beam and the radial grating spokes number are equal, say $l = \pm m$, intensity on the optical axes of the Fraunhofer pattern gets an absolute maximum value and for the other cases, $l \neq \pm m$, the intensity value on the optical axes remains zero. This feature can be used in optical communication. For this purpose, information can be coded on a train of temporally-structured light beam that is formed by switching between two vortex beams having different TC values of l_1 and l_2, and decoding can be done by measuring the intensity values on the optical axis when the train of the light beam is diffracted from an amplitude radial grating having an m equal to l_1 or l_2. In other words, an alteration between two vortex beams in the input plane is translated to a binary change in the intensity of the output light on the optical axis, in real time.

Another interesting result is the accessing to an intense and wide-length light-bar on the optical axis that might find other applications, for example, this needle-like optical beam could be used in particle trapping [24], fluorescence microscopy [25, 26], and material processing [27].

In Fig. 5, for different propagation distances, the intensity profiles along a radial line over the calculated diffraction patterns are illustrated. In all plots, the intensities are normalized to the maximum value of the intensity over the resulted diffraction pattern. We see that, for $|l| \neq m$, at all propagation distances, the value of the intensity on the optical axis remains zero. Also for the case $|l| = m$ we see that, the intensity on the optical axis immediately gets a locally maximum value, by increasing the propagation distances its value increases, and after a given propagation distance its value gets absolute maximum. This transition from a locally to an absolute maximum intensity for different values of ms and ls are shown in Fig. 6(a). It is shown that, the least prorogation distance in which the intensity on the optical axis becomes absolute maximum, increases by increasing values of m and l. The efficiency of conversion of power of incident vortex beam into on-axis spot when $m = l$ can be determined by using the calculated Fraunhofer diffraction pattern for different values of m.

4. ON-AXIS SPOT FORMATION

In the following we show that, the on-axis spot is obtained when m of the radial amplitude grating is same as the order of the beam's topological charge. In addition, we show that how the intensity value is zero when $m \neq |l|$.

By replacing $R' = (\frac{\pi w r}{\lambda z})^2$ and $\psi_F = \frac{e^{i(l\theta+kz)}}{4i}(\frac{w}{r})e^{-\frac{R'}{2}}$ in Eq. 19 we get

$$\psi(r,\theta,z) = \psi_0\left(\frac{e^{-R'/2}}{\sqrt{R'}}\right) \left[2(-i)^{|l|}R'^{s}e^{-R'/2} + \Gamma_+ M_{s,\frac{m+l}{2}}(R') + \Gamma_- M_{s,\frac{m-l}{2}}(R')\right], \quad (24)$$

where $\psi_0 = \frac{z_0 e^{i(\alpha r^2+l\theta+kz)}}{16\pi i z}$. This equation presents the Fraunhofer diffraction when $|l| \leq m$. The Whittaker function $M_{\mu,\nu}(x)$ can be expressed in terms of the Kummer function (of the first kind) $M(a,b,x) = {}_1F_1(a;b;x)$ as follow [28]:

$$M_{\mu,\nu}(x) = e^{-x/2}x^{\nu+1/2}M(\nu-\mu+\frac{1}{2}, 2\nu+1, x). \quad (25)$$

Now, using this expression, Eq. 24 can be rewritten in the following form:

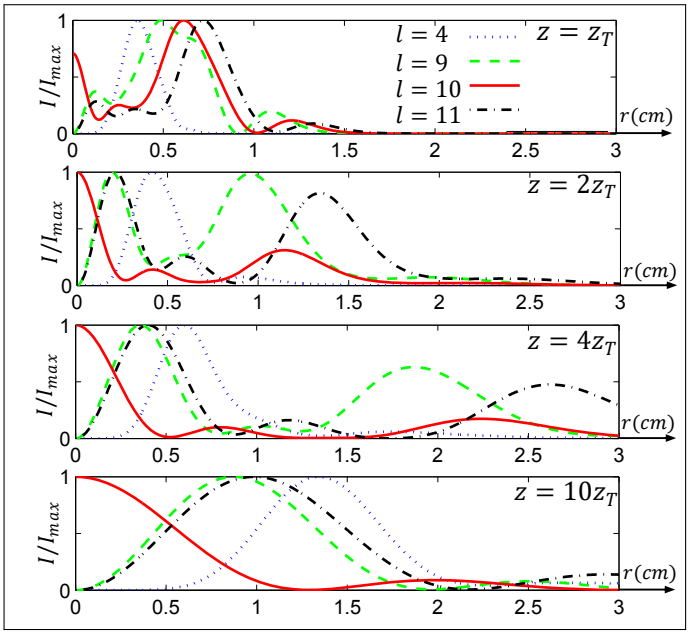

Fig. 5. Normalized intensity profiles along a radial line over the calculated diffraction patterns resulted by passing of different vortex beams with $l = 4, 9, 10, 11$ through an amplitude radial grating with $m = 10$. Plots at different rows are correspond to different propagation distances.

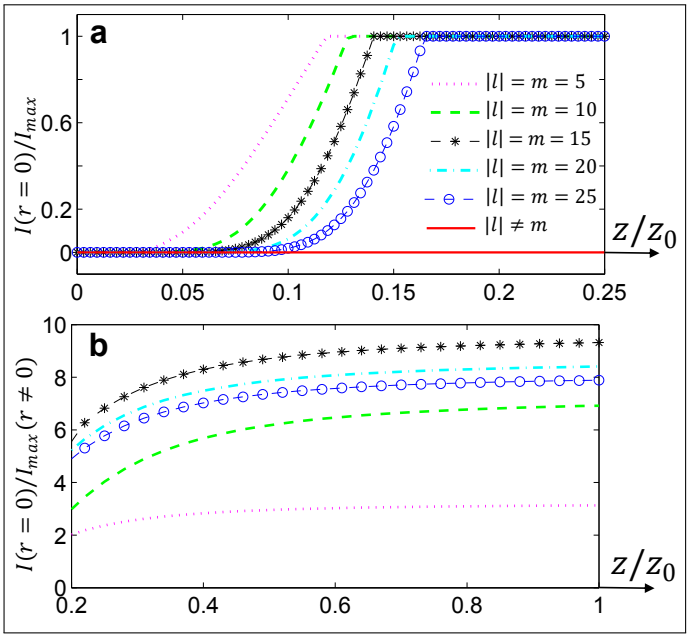

Fig. 6. (a) Normalized intensities on the optical axis over the calculated diffraction patterns resulted by passing of different vortex beams through different amplitude radial gratings with various m and l combinations, (b) ratio of on-axis intensity to the out-of-axis local maximum intensity in terms of the propagation distance for the same values of m used in (a). The plot legends in (b) are the same of (a).

$$\psi(r,\theta,z) = \psi_0 e^{-R'}\{2(-i)^{|l|}R'^{|l|/2} + \Gamma_+ R'^{\frac{m+l}{2}} M(a_+,b_+,R') + \Gamma_- R'^{\frac{m-l}{2}} M(a_-,b_-,R')\}, \quad (26)$$

where $a_\pm = \frac{m\pm l-|l|}{2}$ and $b_\pm = m \pm l + 1$. The behavior of the diffracted light beam on the optical axis can be explained easily by this equation. On the optical axis $R' = 0$ and as $M(a,b,0) = 1$, Eq. 26 explicitly shows that the light beam amplitude vanishes on the optical axis, unless the case $l = \pm m$. For the case $l = \pm m$, one of the second or third terms is non-zero and therefore the light beam amplitude on the optical axis gets a non-zero value. Thus on-axis spot formation is mathematically explained.

From two points of views the focusing behavior of the beam into the on-axis spot can be investigated. In the following, we discuss on the reliability of the method for discrimination of two modes of vortex beams with $m = l$ and $m \neq l$. Also, we define and calculate power conversion efficiency by the ratio of power converted into the on-axis spot to the whole beam power. In some potential applications value of this efficiency would be important. The proposed method in principle has a high value of reliability for discrimination of two modes of vortex beams with $m = l$ and $m \neq l$. As is shown above for the case $m \neq l$, the intensity value over the optical on-axis in theory is zero and in the measurement is equal to the dark noise of the detection system. Therefore, a vortex beam with $m = l$ is discriminable from another beam with $m \neq l$ when the measured value of the intensity over the on-axis spot to be greater than the dark noise. This condition is accessible very easily. In Fig. 6(b) calculated ratio of on-axis intensity, $I(r = 0)$, to the out-of-axis local maximum intensity, $I_{max}(r \neq 0)$, in terms of propagation distance for the different values of m are illustrated. As is apparent the value of on-axis intensity is several times greater than the value of out-of-axis local maximum intensity. This fact guarantees that for the case of $m = l$ the intensity over the optical axis is very greater than the dark noise. We have also calculated the power conversion efficiency defined by the ratio of power converted into the on-axis spot to its total value. In Fig. 7 calculated power conversion efficiency for different values of m are shown. These calculated values are remarkably greater than the efficiency of the sorting of orbital angular momentum states of light with the hologram based detection methods when a large number of modes are detected simultaneously [29–31].

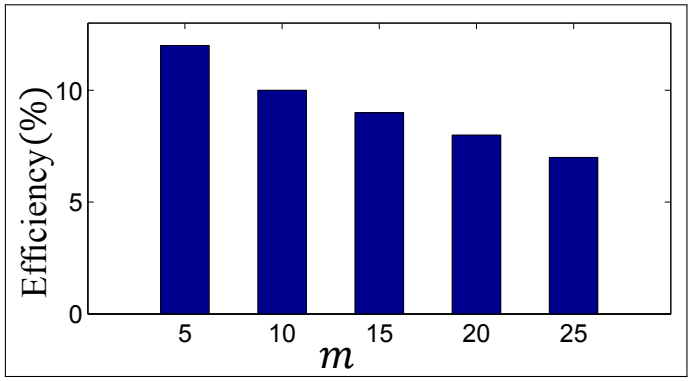

Fig. 7. Calculated efficiency of the power conversion into the on-axis spot when $m = |l|$ for different values of m at the Fraunhofer regime.

Another interesting physical effect is the generation of petal-

like beams when $m = 2|l|$ (see Fig. 4 second column, third row). We believe that this interesting effect also might find applications in laser beam manipulations and laser printing, optical communications, and so on. This topic is under study, and corresponding detail mathematical analysis and its results will be published elsewhere.

Furthermore, it seems that by rotating the radial gratings some interesting effects such as a frequency shift for the vortex beams passing through the radial gratings can be observed [32].

5. EXPERIMENTAL WORKS AND RESULTS

We have examined the proposed method experimentally by impinging different vortex beams on a number of amplitude radial gratings. Schematic diagram of the experimental setup is shown in Fig. 8. We produced vortex beams via a conventional SLM. The amplitude radial gratings' structures were constructed by a lithography method on transparent plates with a spatial resolution of 1200 dpi. In the experiment, a collimated wavefront of a He–Ne laser passes through the SLM and resulted first order diffraction beam is used as a votex beam. It passes through the radial grating. By using a lens, we get both Fresnel and Fraunhofer diffraction patterns by a suitable magnification on a CCD camera. Different propagation distances are adjusted by displacing the CCD camera along optical axis. The Fraunhofer diffraction pattern is recorded by the CCD when its sensitive area is placed at the vicinity of the focal plane of the lens. In Fig. 4, second and fourth rows, show the experimentally recorded Fraunhofer diffraction patterns from two amplitude radial gratings having three different spokes numbers of $m = 5, 10$ illuminated by different vortex beams.

By getting away from the focal plane of the lens, the Fresnel patterns with desired magnification are decoder. In Fig. 9, recorded near-field diffraction patterns of two amplitude radial gratings with $m = 10, 15$ in the illuminating by the vortex beams having different l are shown. These results verify all above-mentioned calculated predictions. We see that for the cases $|l| = m = 10$ and $|l| = m = 15$ intensities on the optical axis are locally maximum but for other cases they are zero.

In summery, we showed that the Fresnel diffraction of a vortex beam from a given amplitude radial grating visualizes the TD of the beam and by trying a set of gratings with different spokes numbers, again visually the TC can be determined.

Also, we showed that based on the Fraunhofer diffraction of vortex beams from amplitude radial gratings, an alteration between two vortex beams in the input plane can be translated in real time to a binary change in the intensity of the output light on the optical axis.

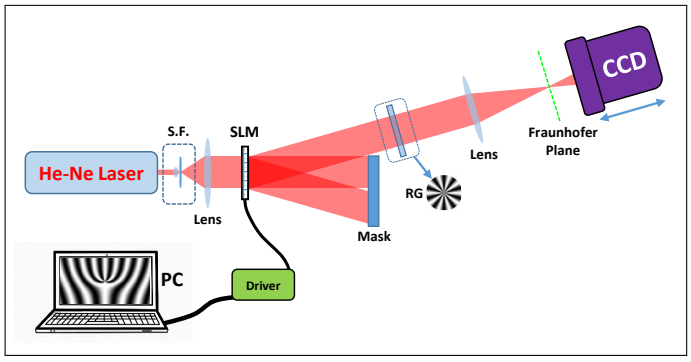

Fig. 8. Schematic diagram of the experimental setup.

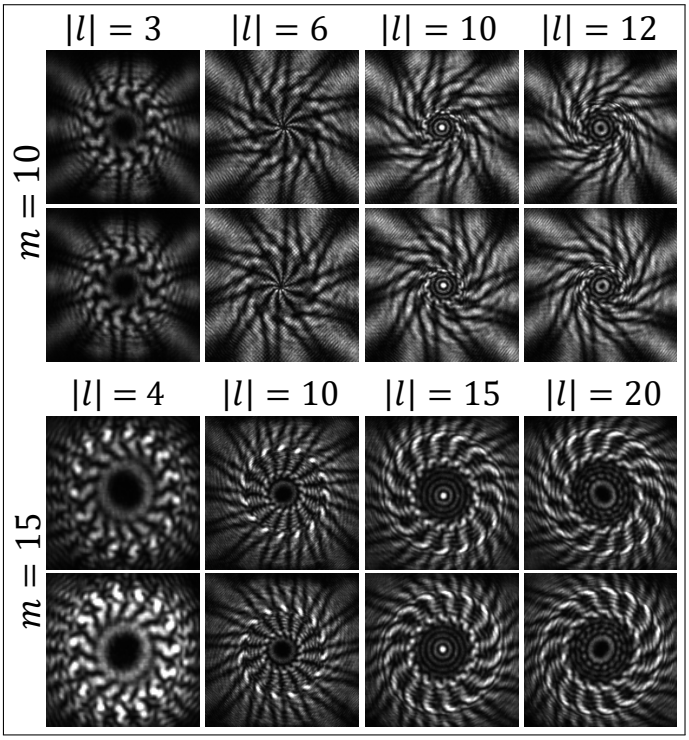

Fig. 9. Experimentally recorded near-field diffraction patterns of two amplitude radial gratings with $m = 10, 15$ in the illumination by the vortex beams having different values of l. First and third rows are for positive l and second and forth rows for the negative values of l.

6. CONCLUSION

We presented a simple, real-time, and calculate-free method for determining TC and TD of the optical vortex beams. The TD for a given vortex beam can be visually determined by the deflection induced on the spokes of a given amplitude radial grating at the near-field diffraction. When radial grating's spokes number is equal to the TC of the beam, intensity over the optical axis is maximum, therefore an alteration between two vortex beams with $|l| = m$ and $|l| \neq m$ can be translated to a binary change in intensity of the output light. Presented method can be used in optical communications.

ACKNOWLEDGMENTS

We acknowledge partial supports from Iran National Science Foundation (INSF) under grant No. 95001286 and IASBS Research Council under grant No. G2017IASBS12632.

REFERENCES

1. K. T. Gahagan and G. A. Swartzlander, "Optical vortex trapping of particles," Opt. Lett. 21, 827-829 (1996).
2. A. E. Willner, H. Huang, Y. Yan, Y. Ren, N. Ahmed, G. Xie, C. Bao, L. Li, Y. Cao, Z. Zhao, J. Wang, M. P. J. Lavery, M. Tur, S. Ramachandran, A. F. Molisch, N. Ashrafi, and S. Ashrafi, "Optical communications using orbital angular momentum beams," Adv. Opt. Photon. 7, 66-106 (2015).
3. M. F. Andersen, C. Ryu, P. Cladé, V. Natarajan, A. Vaziri, K. Helmerson, and W. D. Phillips, "Quantized rotation of atoms from photons with orbital angular momentum," Phys. Rev. Lett. 97, 170406 (2006).
4. J. Leach, Jonathan, J. Courtial, K. Skeldon, S. M. Barnett, S. Franke-Arnold, and M. J. Padgett, "Interferometric methods to measure orbital

and spin, or the total angular momentum of a single photon," Phys. Rev. Lett. 92, 013601 (2004).
5. M. Yeganeh, S. Rasouli, M. Dashti, S. Slussarenko, E. Santamato, and E. Karimi, "Reconstructing the Poynting vector skew angle and wavefront of optical vortex beams via two-channel moiré deflectometery," Opt. Lett. 38, 887–889 (2013).
6. P. Panthong, S. Srisuphaphon, A. Pattanaporkratana, S. Chiangga, and S. Deachapunya, "A study of optical vortices with the Talbot effect," J. Opt. 18, 035602 (2016).
7. I. Moreno, J. A. Davis, B. M. L. Pascoguin, M. J. Mitry, and D. M. Cottrell, "Vortex sensing diffraction gratings," Opt. Lett. 34, 2927-2929 (2009).
8. Sh. Zheng and J. Wang, "Measuring Orbital Angular Momentum (OAM) States of Vortex Beams with Annular Gratings," Scientific reports 7, 40781 (2017).
9. L. Janicijevic, S. Topuzoski, L. Stoyanov, and A. Dreischuh, "Diffraction of a Gaussian beam by a four-sector binary grating with a shift between adjacent sectors," Optics Communications 389, 203-211 (2017).
10. C. S. Guo, L. L. Lu, and H. T. Wang, "Characterizing topological charge of optical vortices by using an annular aperture," Opt. Lett. 34, 3686-3688 (2009).
11. Y. Han and G. Zhao, "Measuring the topological charge of optical vortices with an axicon," Opt. Lett. 36, 2017-2019 (2011).
12. B. Khajavi and E. J. Galvez, "Determining topological charge of an optical beam using a wedged optical flat," Opt. Lett. 42, 1516-1519 (2017).
13. R. Chen, X. Zhang, Y. Zhou, H. Ming, A. Wang, and Q. Zhan, "Detecting the topological charge of optical vortex beams using a sectorial screen," Applied Optics 56, 4868-4872 (2017).
14. H. Ma, X. Li, y. Tai, H. Li, J. Wang, M. Tang, Y. Wang, J. Tang Z. Nie, "In situ measurement of the topological charge of a perfect vortex using the phase shift method," Opt. Lett. 42, 135-138 (2017).
15. C. Paterson, "Atmospheric turbulence and orbital angular momentum of single photons for optical communication," Phys. Rev. Lett. 94, 153901 (2005).
16. M. P. J. Lavery, D. J. Robertson, A. Sponselli, J. Courtial, N. K. Steinhoff, G. A. Tyler, A. E. Willner, and M. J. Padgett, "Efficient measurement of an optical orbital-angular-momentum spectrum comprising more than 50 states," New Journal of Physics 15, 013024 (2013).
17. S. Rasouli, A. M. Khazaei, and D. Hebri, "Talbot carpet at the transverse plane produced in the diffraction of plane wave from amplitude radial gratings," J. Opt. Soc. Am. A 35, 55–64 (2018).
18. K. S. Gupta, A. Basuray, S. K. Sarkar, A. Ghosh, and D. K. Basu, "Self-imaging of a sector like radial grating," Optik 84(5), 149–152 (1990).
19. J. Alonso and E. Bernabeu, "Spatial evolution of Gaussian beams diffracted by radial gratings," Opt. Comm. 98, 323–330 (1993).
20. J. Alonso and E. Bernabeu, "Use of effective focal lengths to describe laser-beam evolution after diffraction in radial gratings," J. Opt. Soc. Am. A 10, 1963–1970 (1993).
21. M. Yeganeh and S. Rasouli, "Investigation of the moiré patterns of defected radial and circular gratings using the reciprocal vectors approach," J. Opt. Soc. Am. A 33, 416-425 (2016).
22. J. W. Goodman, Introduction to Fourier Optics, 2nd ed (Singapore: Mcgraw-Hill, 1996).
23. A Jeffrey and D. Zwillinger, eds. Table of integrals, series, and products (Academic Press, 2007).
24. H. Wang, L. Shi, B. Lukyanchuk, C. Sheppard, and C.T. Chong, "Creation of a needle of longitudinally polarized light in vacuum using binary optics," Nature Photonics 2(8), 501–505 (2008).
25. L. Liu, C. Liu, W. C. Howe, C. J. R. Sheppard, and N. Chen, "Binary-phase spatial filter for real-time swept-source optical coherence microscopy," Opt. Lett. 32, 2375-2377 (2007).
26. E. J. Botcherby, R. Juškaitis, and T. Wilson, "Scanning two photon fluorescence microscopy with extended depth of field," Optics communications 268(2), pp.253-260 (2006).
27. K. Kitamura, K. Sakai, and S. Noda, "Sub-wavelength focal spot with long depth of focus generated by radially polarized, narrow-width annular beam," Opt. Express 18, 4518-4525 (2010).
28. G. B. Arfken, Mathematical Methods for Physicists 3nd (Academic Press, 1985).
29. G. C. Berkhout, M. P. Lavery, J. Courtial, M. W. Beijersbergen, and M. J. Padgett, "Efficient sorting of orbital angular momentum states of light," Physical review letters 105, 153601 (2010).
30. G. Gibson, J. Courtial, M. J. Padgett, M. Vasnetsov, V. Pas'ko, S. M. Barnett, and S. Franke-Arnold, "Free-space information transfer using light beams carrying orbital angular momentum," Opt. Express 12, 5448-5456 (2004).
31. S. N. Khonina, V. V. Kotlyar, R. V. Skidanov, V. A. Soifer, P. Laakkonen, and J. Turunen, "Gauss–Laguerre modes with different indices in prescribed diffraction orders of a diffractive phase element," Optics communications 175, 301–308 (2000).
32. J. Courtial, K. Dholakia, D. A. Robertson, L. Allen, and M. J. Padgett, "Measurement of the rotational frequency shift imparted to a rotating light beam possessing orbital angular momentum," Physical review letters 80, 3217 (1998).